Comparison of matched BOLD and FAIR 4.0T-fMRI with [^{15}O]water PET brain volumes

M. R. Zaini, S. C. Strother, J. R. Anderson, and J.-S. Liow
Department of Radiology, University of Minnesota, Minneapolis, Minnesota 55455 and PET Imaging Center, Veterans Affairs Medical Center, Minneapolis, Minnesota 55417

U. Kjems
Department of Mathematical Modeling, Technical University of Denmark, DK-2800 Lyngby, Denmark

C. Tegeler and S.-G. Kim
Center for Magnetic Resonance Research, Department of Radiology, University of Minnesota, Minneapolis, Minnesota 55455

(Received 10 June 1998; accepted for publication 14 May 1999)

Valid comparisons of functional activation volumes from fMRI and PET require accurate registration, matched spatial resolution, and if possible matched noise. We coregistered 4.0T-fMRI and PET volumes, using a series of linear and nonlinear transformations applied to the PET volumes. Because of the limited number of fMRI slices that were available, PET volumes were transformed to the fMRI space. Since 4.0T-fMRI and 4.0T-MRI volumes have significant spatial distortion due to magnet inhomogeneities, high resolution 1.5T-MRI volumes were nonlinearly transformed to 4.0T-MRI volumes as part of the transformation chain. The smoothing effects of these registration transformations were measured, in order to match the spatial resolution of the coregistered fMRI and PET volumes. Spatial resolution of the transformed PET volumes in the fMRI space was degraded by up to 60% due to the transformation process. Due to both the image acquisition characteristics and the coregistration process, the transformed PET volumes had a spatial resolution that was lower than that of fMRI. Therefore, significant smoothing of fMRI volumes was necessary to match their spatial resolution with that of the transformed PET volumes. Matching the spatial resolution of the fMRI volumes to those of the transformed PET volumes was achieved by matching the shape of their point spread functions. In order to do this, Gaussian kernels were employed to smooth the fMRI volumes. We were unable to simultaneously match the resolution and noise of fMRI and PET signals in the motor cortex. Activation maps derived from transformed PET and smoothed fMRI volumes were compared. Contralateral motor cortex was active in all modalities but there were large variations in the size of the activated region and its signal to noise ratio across BOLD, FAIR, and PET images within each subject. Nevertheless, the relative CBF changes measured by FAIR were consistent with those determined by PET. [S0094-2405(99)01608-9]

Key words: PET, fMRI, image transformation, spatial resolution, brain activation

I. INTRODUCTION

Comparison of the two functional brain imaging modalities, PET and fMRI, is the subject of a number of recent investigations.[1–5] This work was performed as part of a comparison of functional activation volumes from [^{15}O]water PET studies and the blood-flow dependent fMRI technique called flow sensitive alternating inversion recovery (FAIR).[5–7] Our investigation differs from the previous studies, in its use of high field MRI and fMRI, the transformation techniques employed, working with both FAIR-fMRI and blood oxygenation level dependent (BOLD) fMRI volumes, and consideration of the impact of all image processing manipulations on spatial resolution of the transformed volumes.

PET and fMRI differ in their reproducibility, signal to noise ratio, contrast, and spatial resolution. There exist many statistical analysis techniques for measuring functional activation maps of the brain.[8,9] In order to compare PET and fMRI, activation maps from any of these statistical models need to be coregistered and their spatial resolution matched. In this work, PET volumes were registered to fMRI volumes, using a series of global rigid body, global affine, and local curved (warping) transformations. The effect of these transformations on the spatial resolution of the PET volumes was measured. Subsequently, the spatial resolution and mean noise levels of the fMRI volumes was matched to that of the transformed PET volumes in the fMRI space. This report deals with (i) the techniques and tradeoffs involved in performing such a match when the fMRI volumes have significant spatial distortion, and (ii) preliminary comparison of the resulting matched FAIR, BOLD, and PET activation volumes for a simple motor task.

fMRI volumes typically have a higher spatial resolution than the PET volumes; so it is better to transform fMRI volumes to the PET space, since the transformation process degrades the spatial resolution and brings the spatial resolution of fMRI volumes closer to that of the PET volumes.

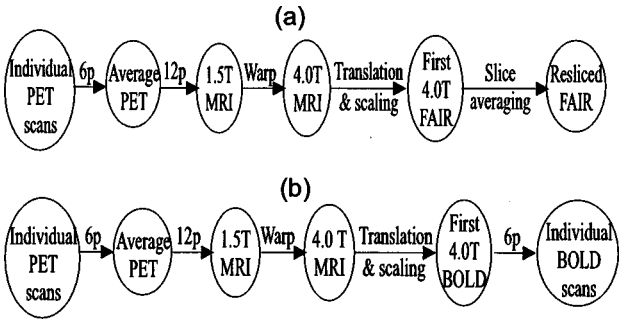

FIG. 1. Set of transformations used in determining the PSF of the warped PET into the fMRI-FAIR (a) and fMRI-BOLD (b) spaces. 6P is 6-parameter global rigid-body transformation, 12P is 12-parameter global affine transformation, and the local warp is based on maximizing voxel similarity measure (see text).

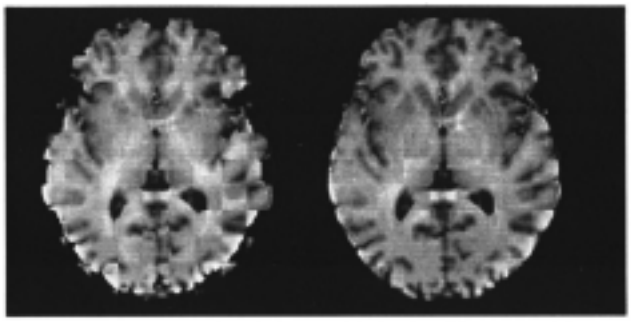

FIG. 2. Comparison of 12P (left) vs warping (right) techniques in registering structural 1.5T-MRI to structural 4.0T-MRI. A checkerboard of alternating squares from the 1.5T- and 4.0T-MRI images is used to depict both 12P and warping registration results.

However, since fMRI volumes using the FAIR technique were acquired only with a limited number of contiguous slabes (3 or 5), PET volumes were transformed to the fMRI space.

II. METHODS

A. Image acquisitions

Four normal volunteers underwent [^{15}O]water PET, whole-brain BOLD 4.0T-fMRI, and FAIR 4.0T-fMRI scanning, while performing a finger-to-thumb opposition task. Eight or ten PET scans were performed on each subject, on a Siemens ECAT 953B scanner in 3D mode, as described by Strother *et al.*[9] In addition, 3 runs of 76 or 84 BOLD scans (analyzed in Tegeler *et al.*[10]) and 50 or 70 FAIR scans were performed on each subject. BOLD-fMRI volumes were acquired, using a single-shot gradient-echo EPI technique, on 34 coronal slices covering the whole brain. The parameters for BOLD-fMRI were a matrix size of 64×64, a FOV of $24\times24\,\mathrm{cm}^2$, a slice thickness of 5 mm, TE of 25 ms, and TR of 5 s.[5] BOLD images were acquired coronally because axial acquisition introduces significant acoustic noise due to the gradient hardware of our 4.0T scanner. Therefore, whenever possible, we acquire images coronally, especially for whole brain studies. In FAIR-fMRI, three-slice images were acquired within a 1.5 cm thick slab covering the primary motor areas (TI=1.4 s, TR=2.95 s, and inversion slab=2.5 cm).[5] FAIR images were acquired axially, since arterial blood flows in the inferior–superior direction.

T1-weighted structural 1.5T- and 4.0T-MRI studies were also performed on these subjects. The structural MRI images were acquired using the 3D imaging sequence, ''modified driven equilibrium Fourier transform (MDEFT).''[11] The parameters were a matrix size of $128\times128\times64$, FOV of $24\times24\times18\,\mathrm{cm}^3$, TE of 3 ms, TR of 7 ms, number of segments of 4, and tau of 1.3 s.

B. Spatial transformation of volumes

Individual PET volumes for each subject were transformed to the fMRI space using the set of transformations in Fig. 1. In Fig. 1, 6P refers to 6-parameter global rigid body transformation using the AIR code,[12] 12P refers to 12-parameter global affine transformation, and the local warp was done using the code of Kjems *et al.*[13] The warp code employed in this work was based on a hierarchically scaled search for a displacement field maximizing one of several voxel similarity measures derived from the two-dimensional histogram of matched image intensities subject to a regularizer that ensures smoothness in the displacement field. The optimization technique for the global voxel similarity measure employed in this work was based on the local least squares method. The warping calculations between the structural 1.5T- and 4.0T-MRI scans were initialized by a 12P transformation matrix. Warping registered the 1.5T-MRI images more closely to the 4.0T-MRI images than the 12P method did. The quality of the warp vs the 12P registration techniques can be inspected visually in Fig. 2. The images in Fig. 2 are displayed using a checkerboard template, where the first moments of the structural 4.0T-MRI, 12P-transformed 1.5T-MRI, and warped 1.5T-MRI are matched.

The individual PET scans were registered (6P) to the first PET scan for each subject. An average PET scan, in the first PET scan space, was formed and used in calculating the 12P transformation matrix between itself and the 1.5T structural MRI volume. The rigid body transformation between structural 4.0T-MRI and 4.0T-FAIR fMRI in Fig. 1(a) was computed only based on global scaling and translation, because the limited number of FAIR slices were not suitable for implementing either AIR or the 12P techniques. Hence, using the first FAIR scan, instead of an average FAIR scan, was adequate. Furthermore, the limited number of slices in the FAIR volumes did not allow the computation of intramodality transformation matrices of the FAIR scans. This did not cause any problems, since the maximum head motion during the acquisition of FAIR volumes was visually checked and found to be negligible.

The acquisition of EPI-fMRI images on the 4.0T scanner introduces significant spatial distortion; hence incorporating the undistorted 1.5T-MRI volumes into the transformation process was found to be essential. The reason for the last slice averaging step in Fig. 1(a) was to better match the transformed PET and will be explained in more detail in Sec. III C.

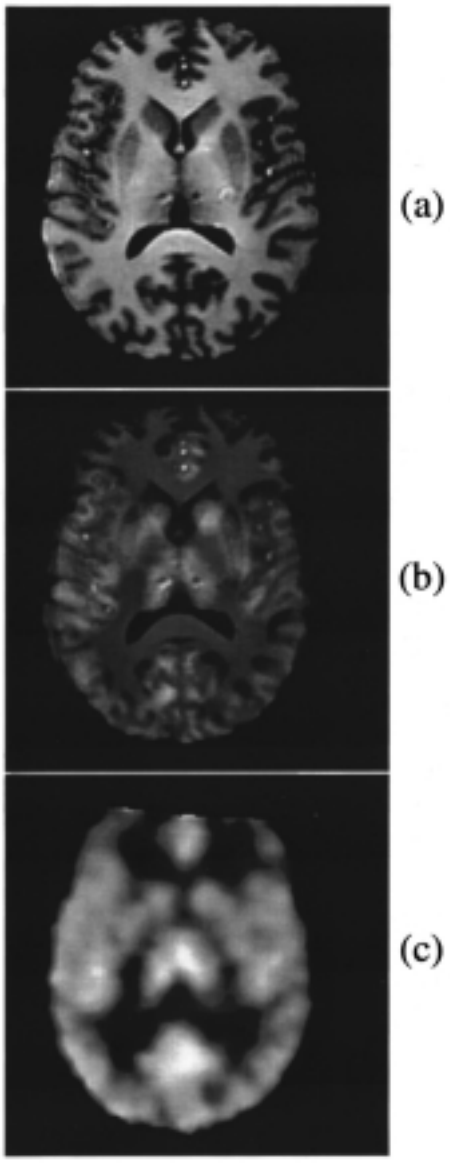

FIG. 3. (a) A 4.0T-MRI slice, (c) transformed PET image to the 4.0T-MRI space for the same subject, (b) superposition of (a) and (c) to show the accuracy of spatial transformations.

All the above transformations were combined and applied to the individual PET volumes in one step, so that resampling, performed using sinc interpolation and sampling, would be done on the volumes only once. An example of a PET image registered to a structural 4.0T-MRI image is shown in Fig. 3. The registration quality for a PET image registered to an fMRI image cannot be easily assessed visually, since they both have lower spatial and contrast resolution than structural MRI images and the spatial extent of the fMRI images is limited. Therefore, a coregistered PET and structural 4.0T-MRI image is shown in Fig. 3. Figure 3(a) is a slice of a structural 4.0T-MRI, Fig. 3(c) is a PET image transformed to the 4.0T-MRI space, and Fig. 3(b) is a screen-door superposition of the two.[14]

For the PET-BOLD case—like the PET-FAIR case—only global scaling and translation could be used for the transformation between 4.0T-MRI and 4.0T-BOLD [Fig. 1(b)]. But, for this case, the unsuitability of BOLD images (e.g., the existence of large magnetic susceptibility artifacts for the tissue–air interfaces) was the reason for the inability to register them to the 4.0T-MRI volumes using the AIR or the 12P techniques. Employing the first BOLD scan, instead of an average BOLD scan, for finding a global scaling and translation transformation matrix sufficed because the individual BOLD scans of all three runs were registered to the first BOLD scan, using the 6P rigid body transformation. Based on these intramodality transformation matrices, the maximum and average motion recorded in any brain voxel during the BOLD-fMRI acquisitions was determined to be less than 2 mm and 1 mm, respectively, for all four subjects.

C. PSF determinations

In order to measure the effect of these transformations on the transformed PET images in the fMRI space, the point spread function (PSF) of the entire process in Fig. 1 was determined. Since the goal was to match the spatial resolution of the individual PET scans to that of the individual fMRI scans, the transformation process includes the intramodality matrices. In Fig. 1, the average intramodality transformation matrix for all of the PET scans of a single subject was used for the first transformation step in determining the process PSF. This is conceptually equivalent to creating an average PET volume.

For the PET-BOLD case compared to the PET-FAIR case, an extra 6P transformation matrix was applied in determining the PSF of the entire registration process, as shown in Fig. 1(b). This additional transformation matrix was the average of all of the three runs of 76 or 84 intrasubject, intramodality transformation matrices for the BOLD scans. This average transformation matrix was almost a unity matrix, indicating that motion was indeed insignificant. For the PET-FAIR case, however, the intramodality transformation for the FAIR scans could not be calculated, as explained earlier.

Determining the PSF of the transformation sequences that take the individual PET scans into the fMRI space was initiated by measuring multiple point sources in a phantom.[15] The sources were made of capillary tubes of 0.08/0.11 mm (i.d./o.d.)$\times$90 mm containing high concentrations of ^{18}F. These sources were scanned in the PET scanner, and the images were reconstructed. The source tubes were placed in the scanner, such that their cross sections were perpendicular and parallel to the axial direction, in order to determine the axial and transaxial resolution of the PET scanner, respectively. 3D PET scans of these sources were acquired and their images were reconstructed, using the 3D reprojection-reconstruction algorithm (3DRP), while applying a Hanning filter in the transaxial direction only.[15]

Since all of the PET image volumes were scanned off-center in the FOV of the PET scanner, some of the selected points for the transformation process were outside the measured volume in which the reconstructed PSF was determined. The reconstructed PSF's of such points were calculated by extrapolating the full-width at half-maximum

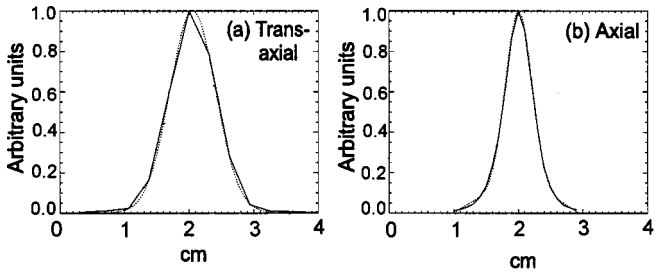

FIG. 4. Spatial resolution profiles of reconstructed PET volumes. Solid curves are the measured values and the dotted curves are the fitted Gaussians.

(FWHM) of the measured points. The extrapolation method used was that of fitting an exponential curve through the available measured data points.

The fitted Gaussians for 3 to 7 reconstructed PSF profiles, per subject, at various points in the PET volume were passed through the transformation steps in registering both PET to FAIR and PET to BOLD volumes. These points were selected so that they would be representative of the whole volume. Since the FAIR volumes had a limited number of slices, not every starting point in the PET volumes was transformed into the FAIR slices. In order to find which starting points in the PET volumes ended up in the FAIR slices, an inverse mapping method was used. Since the warp field was not invertible at the time of this work, a 12P transformation matrix between 4.0T-MRI and 1.5T-MRI was used instead, as an approximate inverse mapping process.

D. Generating brain activation maps

Since fMRI studies had many more scans in each run compared to PET studies, pseudo-PET volumes were created from the fMRI volumes by averaging all volumes to yield six averaged scans per session. All data were analyzed by a paired *t*-test using an individual variance for each voxel. Mean differences between resting and activation periods and their standard deviation were calculated on a voxel-by-voxel basis. Pooled variance was also calculated by averaging the individual variances of each voxel,[16] which yields more reproducible brain activation maps.[17] Activation maps were generated by thresholding *t*-values corresponding to an uncorrected significance of $p<0.05$. The impact of smoothing the PET volumes in order to match the variance within an anatomically defined volume-of-interest (VOI) covering the contralateral motor area to that of the fMRI volumes was also studied. Transformed PET volumes were smoothed with Gaussian kernels of varying FWHM until mean standard deviation within the VOI was close to that of smoothed fMRI volumes.

III. RESULTS AND DISCUSSION

A. PSF of transformed PET volumes

Figure 4 shows the PSF of the detection and reconstruction operation, for a source at the center of the FOV of the PET scanner. These reconstructed profiles were fitted with Gaussians. The FWHM of the fitted Gaussians are 0.84 cm in the transverse plane [Fig. 4(a)] and 0.52 cm in the axial direction at the center of the FOV of the PET scanner [Fig. 4(b)]. The average of the reconstructed PSF profiles for points in the image volume of each subject is given in Table I.

Three-dimensional Gaussians, having profiles similar to those in Fig. 4 and residing on a uniform volume having the same dimensions as the PET volumes were passed through the transformation processes in Fig. 1. Gaussians were fitted to the resulting profiles of the transformation processes, by minimizing the RMS error between the fitting curves and the

TABLE I. FWHM and standard deviation (of the FWHM) of the original reconstructed PET volumes and the transformed PET volumes in fMRI space. All values are in centimeters.

		Reconstructed PET PSF used for the PET-FAIR case	Transformed PET PSF in the FAIR space		Maximum FWHM increase for PET-FAIR for each subject	Reconstructed PET PSF used for the PET-BOLD case		Transformed PET PSF in the BOLD space		Maximum FWHM increase for PET-BOLD for each subject
		FWHM	FWHM	σ		FWHM	σ	FWHM	σ	
Subject 1	*x*	0.846	0.945	0.029	15%	0.859	0.025	0.987	0.020	38%
	y	0.846	0.789	0.026		0.859	0.025	0.816	0.032	
	z					0.618	0.033	0.836	0.039	
Subject 2	*x*	0.852	0.984	0.092	34%	0.870	0.026	0.959	0.075	60%
	y	0.852	0.744	0.042		0.870	0.026	0.805	0.072	
	z					0.668	0.072	0.938	0.144	
Subject 3	*x*	0.846	0.942	0.128	20%	0.863	0.027	0.977	0.041	51%
	y	0.846	0.725	0.052		0.863	0.027	0.781	0.058	
	z					0.622	0.042	0.864	0.046	
Subject 4	*x*	0.892	1.026	0.051	19%	0.867	0.026	0.968	0.057	34%
	y	0.892	0.839	0.046		0.867	0.026	0.764	0.062	
	z					0.651	0.062	0.789	0.092	

transformed profiles. The FWHM of the transformed PET volumes averaged over all points for each subject is given in Table I. The FWHM of the transformed PET images were measured in the three Cartesian axes of the fMRI-FAIR and fMRI-BOLD spaces. A direct comparison of these FWHM values with those of the reconstructed PSF profiles is not totally accurate, since the latter are in the original PET space, whereas the transformed PET are in the fMRI space. In other words, the original PET, fMRI-FAIR, and fMRI-BOLD volumes are all in different spaces. The only statement that can be made regarding the effect of the transformation processes on the spatial resolution of the PET volumes is on the maximum PSF profile widening. As it can be seen in Table I, the maximum spatial resolution degradation of the PET volumes is 34% for the PET-FAIR transformation process in the transverse plane. The FWHM of the transformed PET in the resliced FAIR space (to be explained in Sec. III C) in the axial direction (z-direction) is not cited in Table I, since the transformed PET volumes in that space have been sampled at only 2 or 4 points. Such low sampling is not enough for an accurate estimate of the PSF. Furthermore, the standard deviation of the FWHM values of the first data column in Table I is almost zero, since in order for the transform of these points to lie in the limited 2–4 slices of the FAIR space, they had to reside in close proximity of each other in the original PET space. The maximum widening in the PSF of the PET volumes upon being transformed to the BOLD space is 20% in the transverse plane and 60% in the axial direction (z-direction). The reason PSF degradation is larger in the axial direction is the coronal slice acquisition of the fMRI-BOLD images.

B. PSF of FMRI volumes

fMRI volumes had a FWHM of 0.375 cm in the readout plane and 0.500 cm in the slice selection direction. Spatial resolution profiles of fMRI images were obtained by taking the inverse Fourier transform of the readout sequence and taking the forward Fourier transform of the soft rf pulse, respectively. FWHM of the readout profile (a sinc function) was chosen to be one pixel in the readout plane of fMRI volumes. On the other hand, the width of the slice selection profile (solid line in Fig. 5) had six bins in temporal frequency, corresponding to six spatial bins in the slice selection direction. However, a slice of the fMRI volumes was selected to incorporate four such bins, which corresponds to four data points acquired during fMRI scanning. FAIR volumes were acquired transversely, whereas the BOLD volumes were acquired coronally. BOLD voxels were subsequently resized to a cubic shape (0.375 cm edge), so that the intramodality, intrasubject transformation matrices could be calculated with a uniform voxel size.

Resizing of the voxels in BOLD volumes changed their spatial resolution profile in the slice selection direction from that of the solid line in Fig. 5. The resizing was done using trilinear interpolation. In one dimension, the effect of this type of resizing can be modeled by convolving the solid profile of Fig. 5 with a triangular curve that is two pixels

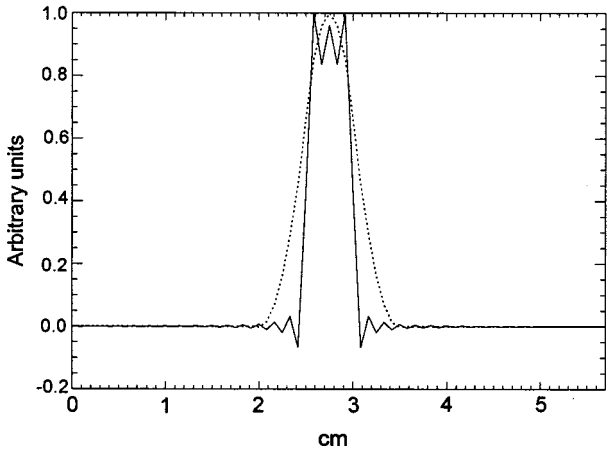

FIG. 5. Spatial resolution profile of fMRI images in the slice selection direction (perpendicular to the coronal plane), before (solid) and after (dotted) voxel resizing. Voxel resizing was done for fMRI-BOLD images only.

wide. The result of this convolution is shown as the dotted profile in Fig. 5. Therefore, the FWHM of the spatial resolution profiles of the BOLD volumes were 0.375, 0.625, 0.375 cm in the three Cartesian directions, after employing trilinear interpolation for voxel resizing. Hence, the spatial resolution of the BOLD volumes in the direction perpendicular to the coronal plane was increased from 0.500 cm to 0.625 cm, due to voxel resizing. However, the FWHM of the spatial resolution profiles of the FAIR volumes remained at 0.375, 0.375, 0.500 cm in the three Cartesian directions, with 0.500 cm being the spatial resolution in the direction perpendicular to the transverse plane.

C. Spatial resolution matching

Matching the spatial resolution of the fMRI images to that of the transformed PET images was accomplished by applying smoothing Gaussian kernels to the fMRI volumes. In other words, spatial resolution profiles of fMRI images (like

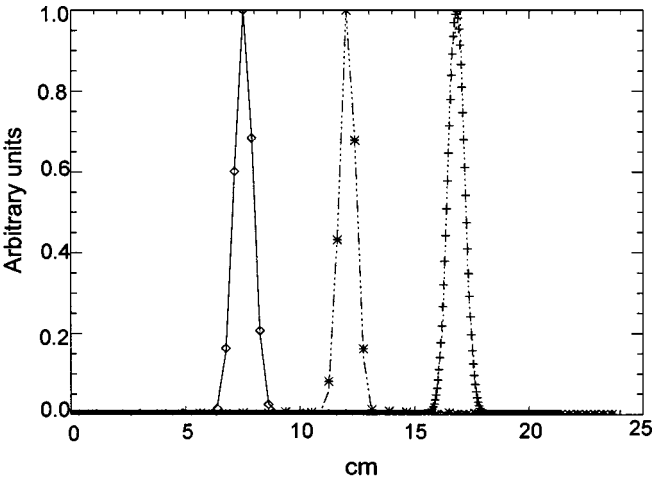

FIG. 6. Spatial resolution profiles of transformed PET in fMRI-BOLD space (curves) and smoothed fMRI-BOLD (symbols) volumes, in the three Cartesian directions.

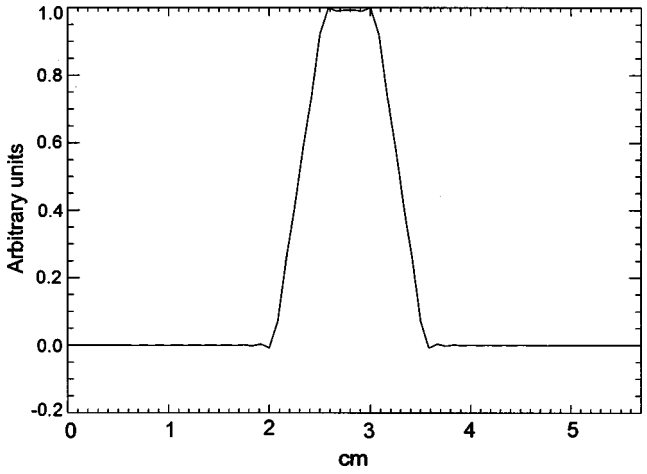

FIG. 7. Axial resolution profile of fMRI-FAIR images, after adjacent slice averaging.

the sinc function in the readout plane and the dotted line in Fig. 5 in the slice-selection direction for the PET-BOLD case) were iteratively convolved with Gaussian kernels to match profiles of the transformed reconstructed PSF of PET volumes. The shape of the smoothing kernels was obtained by optimizing the RMS error between the smoothed PSF of the fMRI images and the PSF of the transformed PET images. In this optimization process, the magnitude and binsize of the convolution operands were matched. Typical matched profiles in the slice selection and readout directions for the PET-BOLD case are shown in Fig. 6.

For the PET-FAIR case, due to the limited number of slices (3 or 5), there were insufficient axial samples to accurately apply smoothing Gaussian kernels. Hence, adjacent slice averages were used to reslice the FAIR images and bring the FWHM of the axial FAIR profile closer to that of the axial profile of the transformed PET volumes. Slice averaging can be modeled as the convolution of the solid profile of Fig. 5 (FAIR was acquired transversely) with a two-slice wide rect. function. The result of this operation is shown in Fig. 7. The FWHM of the profile in Fig. 7 is 1.0 cm. This width is within ± 0.15 cm of the FWHM in the axial direction of the transformed PET volumes in the FAIR space (estimated from the two subjects that had four sample points). Matching the spatial resolution of the FAIR images to those of the transformed PET images in the transverse plane was accomplished in the same manner as in the PET-BOLD case.

TABLE II. FWHM and standard deviation (of the FWHM) of the smoothing Gaussians to be applied to the fMRI volumes, in order to match their spatial resolution with those of the transformed PET volumes in the fMRI space. All values are in centimeters.

		PET-FAIR		PET-BOLD	
		FWHM	σ	FWHM	σ
Subject 1	x	0.949	0.030	0.972	0.024
	y	0.811	0.023	0.610	0.036
	z			0.847	0.027
Subject 2	x	0.966	0.068	0.963	0.070
	y	0.775	0.035	0.568	0.111
	z			0.902	0.089
Subject 3	x	0.947	0.120	0.983	0.040
	y	0.757	0.047	0.549	0.041
	z			0.880	0.041
Subject 4	x	1.011	0.061	0.974	0.053
	y	0.848	0.040	0.558	0.092
	z			0.812	0.081

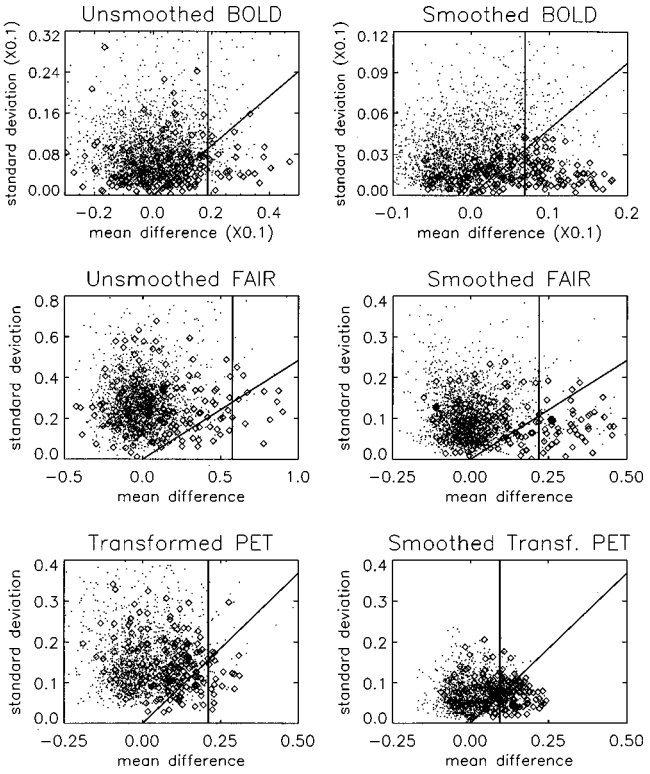

FIG. 8. Scatter plots of the individual-voxel standard deviation of the differences between resting and activation periods vs the mean differences, for subject 1. The sloped and vertical lines correspond to the chosen threshold of $p=0.05$ for the individual and pooled variances, respectively. Dots represent single voxels, and diamonds are voxels identified in the primary motor area.

The FWHM of the smoothing Gaussian kernels, applied to the fMRI images, averaged over all points, for the four subjects are given in Table II. As mentioned earlier, in the axial direction, the FAIR images were resliced, instead of applying smoothing Gaussians. The uncertainties in Tables I and II are not based on an assumed distribution function; hence they reflect the standard deviation of the FWHM values of the sample points from which they were calculated. Voxel resizing of BOLD volumes led to the smoothing Gaussians having a narrower width in the slice selection direction than in the other directions.

D. Brain activation results

Figure 8 shows scatter plots of the standard deviation vs the mean difference of signal intensities between resting and activation periods in unsmoothed and smoothed BOLD,

TABLE III. Mean percent changes in the anatomically defined contralateral motor cortex.

	Smoothed BOLD	Smoothed FAIR	Transformed PET	Smoothed Trans. PET
Subject 1	1.05	14.50	18.55	18.11
Subject 2	0.68	7.81	10.44	10.31
Subject 3	1.08	11.46	16.44	11.00
Subject 4	0.67	11.38	2.24	1.37
Average	0.87	11.29	11.92	10.20

FAIR, and transformed PET. Dots represent individual voxels, and diamonds are those voxels that lie within the anatomically defined contralateral primary motor area. The sloped and vertical lines denote the threshold of $p=0.05$ for the individual and pooled variance techniques, respectively. The individual variance method results in more voxels being selected as activated (to the right of the sloped line) compared to those as activated using pooled variance (to the right of the vertical line). As seen in Fig. 8, matching the spatial resolution of fMRI volumes by employing the Gaussian kernels of Table II results in more voxels in the primary motor area passing the threshold ($p<0.05$) because the noise per voxel (vertical axis) decreases faster than the mean difference signal.

As seen in Fig. 8 and Table III, the mean difference values of the transformed PET and smoothed FAIR, which have matched spatial resolution, have approximately the same motor cortex mean, whereas their noise levels per voxel (or standard deviation) do not. Therefore, a scatter plot of a smoothed PET volume using a 3D Gaussian kernel having a 1.0 cm FWHM is also depicted in the lower right panel. Smoothing the PET volumes matched their mean voxel noise levels in the motor cortex to those of the smoothed fMRI-FAIR volumes (standard deviation=0.8 after smoothing for both FAIR and PET for subject 1 of Fig. 8). Therefore, noise matching led to a mismatch of spatial resolution, which indicates that matching both noise and spatial resolution is not possible in this data set.

Functional maps, created using paired *t*-test, for all four subjects are shown in Fig. 9, where the rows from top to bottom show the activated voxels in the unsmoothed BOLD, smoothed BOLD, unsmoothed FAIR, smoothed FAIR, unsmoothed PET, and smoothed PET. All these volumes are in the FAIR space. Note that the PET data in Fig. 9 do not extend to the posterior rim of the brain because of the limited axial field-of-view of our PET scanner. As seen in Fig. 9, images for which only spatial resolution is matched do not necessarily reflect well matched activation patterns. This is likely due to differences in noise power characteristics and physiology defining the BOLD, FAIR, and PET signal structure. Smoothed PET images, with attempt to match their noise levels to those of the smoothed FAIR images, show primary motor activation patterns that are similar to those of the smoothed FAIR images.

The primary motor activation sites of the smoothed PET and smoothed fMRI volumes are similar, but the medial motor area which is similarly active in the first three subjects (first three columns of Fig. 9) for smoothed BOLD and smoothed PET is largely absent from the smoothed FAIR images. The size of the active area in the contralateral (right) motor cortex is the largest in smoothed BOLD, and more similar in smoothed PET and FAIR. The ipsilateral (left) premotor area was also active in some subjects, which is consistent with our previous observations.[18] In BOLD functional maps, activation at the edge of the brain was seen due to large venous vascular contributions.

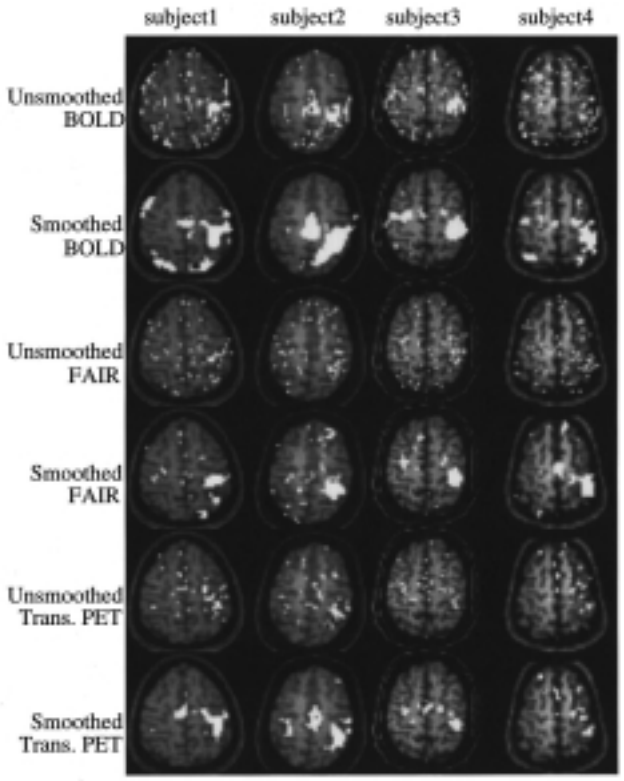

FIG. 9. Activation maps using paired *t*-test for all four subjects. All images are in the FAIR space.

Relative mean signal changes in the motor area as measured by BOLD, FAIR, and PET are shown in Table III. Relative signal changes in PET reflect cerebral blood flow (CBF) changes during the finger opposition task. Since these mean changes in FAIR within the motor cortex agree quite well with those in PET, we conclude that FAIR also reflects relative CBF changes.

IV. SUMMARY

PET volumes of four subjects went through multiple global affine and local warping transformations to register them to fMRI volumes. Measuring and applying smoothing kernels that compensate for the effects of linear and nonlinear registration transformations is an essential part of the comparison of PET and fMRI images. The effect of these transformations on the spatial resolution of reconstructed PET volumes was to increase their FWHM by up to 0.44 cm or 60% for their transformation to the BOLD space and by up

to 0.29 cm (i.e., 34%) for their transformation to the FAIR space. While these increases can be reduced by deliberately choosing acquisition parameters to approximately match multimodality resolution, this leads to nonoptimal fMRI acquisitions. The issue of direct matching will be explored in future studies. The FWHM of the spatial resolution profile of transformed PET volumes was 0.21–0.79 cm (1.4–3.1 times) larger than those of the fMRI volumes. This represents a basic problem in comparing large axial extent PET volumes with limited axial extent fMRI studies. In this work, the minimum smoothing required to match the spatial resolution of coregistered volumes, due to their inherent image acquisition resolution and to the impact of multiple linear and nonlinear transformations, was applied to the volumes which had a finer spatial resolution, namely fMRI volumes.

Gaussian kernels, having FWHM of 0.417–1.079 cm can be applied to the fMRI volumes to match their spatial resolution profile to those of the transformed PET volumes, at different regions of the brain volumes of different subjects. The FWHM of the smoothing Gaussians vary somewhat within an individual subject's volume. Sample standard deviation of these variations range from 0.023 to 0.120 cm; or their coefficient of variation range from 3% to 13%. However, only the mean Gaussian kernel for each subject was chosen for the smoothing of fMRI volumes, in order to match their spatial resolution profile to those of the transformed PET volumes in the fMRI space. In addition to matching the spatial resolution of coregistered volumes, other issues such as matching their noise power need to be addressed and the likely tradeoffs between matching resolution or noise power investigated. Matching the noise power of fMRI and PET is nontrivial, due to their different signal sources and structure. We explored smoothing the PET volumes with Gaussian kernels to bring the standard deviation of the difference between resting and activation images in an anatomically defined primary motor area closer to those of smoothed fMRI-FAIR images.

Activation maps using paired *t*-tests were generated for the transformed PET in the fMRI space and smoothed fMRI volumes. Smoothing the fMRI volumes to match their spatial resolution to that of the transformed PET volumes increased the number of activated voxels in the primary motor area. Furthermore, smoothing the PET volumes to approximately match their noise to those of smoothed FAIR increased the number of activated voxels. While it is not possible to simultaneously match resolution and noise across our PET and fMRI experiments, this may be possible using state-of-the-art PET scanners and/or 1.5T fMRI results. Imaging the motor cortex near the center of the FOV and/or using a state-of-the-art PET scanner will tend to decrease PET noise and increase resolution,[19,20] while using more widely available lower field fMRIs (e.g., 1.5T) will tend to decrease both BOLD and FAIR contrast-to-noise levels. The preliminary agreement between PET and FAIR indicate that both modalities measure relative CBF changes.

ACKNOWLEDGMENTS

We thank the anonymous referees for their suggestions, which have improved our paper. This work was supported in part by the Whitaker Foundation and NIH Grants Nos. MH57180 and RR08079.

[1]N. F. Ramsey, B. S. Kirkby, P. Van Gelderen, K. F. Berman, J. H. Duyn, J. A. Frank, V. S. Mattay, J. D. Van Horn, G. Esposito, C. T. W. Moonen, and D. R. Weinberger, ''Functional mapping of human sensorimotor cortex with 3D BOLD fMRI correlates highly with $H_2{}^{15}O$ PET rCBF,'' J. Cereb. Blood Flow Metab. **16**, 755–764 (1996).

[2]G. Rees, A. Howseman, O. Josephs, C. D. Frith, K. J. Friston, R. S. J. Frackowiak, and R. Turner, ''Characterizing the relationship between BOLD contrast and regional cerebral blood flow measurement by varying the stimulus presentation rate,'' Neuroimage **6**, 270–278 (1997).

[3]N. Sadato, V. Ibanez, G. Campbell, M-P. Deiber, D. Le Bihan, and M. Hallett, ''Frequency-dependent changes of regional cerebral blood flow during finger movements: Functional MRI compared to PET,'' J. Cereb. Blood Flow Metab. **17**, 670–679 (1997).

[4]C. Dettmers, A. Connelly, K. M. Stephan, R. Turner, K. J. Friston, R. S. J. Frackowiak, and D. G. Gadian, ''Quantitative comparison of functional magnetic resonance imaging with positron emission tomography using a force-related paradigm,'' Neuroimage **4**, 201–209 (1996).

[5]S.-G. Kim, S. C. Strother, J.-J. Sidtis, J. R. Anderson, K. Rehm, K. Ugurbil, and D. A. Rottenberg, ''Comparison of functional activation studied by BOLD- and CBF-based fMRI and PET during sequential finger opposition,'' in Proceedings of the International Society of Magnetic Resonance Medicine 5th Science Mtg., Vancouver, Canada, 1997 (unpublished), p. 379.

[6]S.-G. Kim and N. V. Tsekos, ''Perfusion imaging by a flow-sensitive alternating inversion recovery (FAIR) technique: Application to functional brain imaging,'' Magn. Reson. Med. **37**, 425–435 (1997).

[7]S.-G. Kim, N. V. Tsekos, and J. Ashe, ''Multislice perfusion-based functional MRI using the FAIR technique: Comparison of CBF and BOLD effects,'' NMR in Biomedicine **10**, 191–196 (1997).

[8]K. J. Worsley, ''An overview and some new developments in the statistical analysis of PET and fMRI data,'' Human Brain Mapping **5**, 254–258 (1997).

[9]S. C. Strother, J. R. Anderson, K. A. Schaper, J. J. Sidtis, J.-S. Liow, R. P. Woods, and D. A. Rottenberg, ''Principal component analysis and the scaled subprofile model compared to intersubject averaging and statistical parametric mapping. I. 'Functional connectivity' of the human motor system studied with [^{15}O] water PET,'' J. Cereb. Blood Flow Metab. **15**, 738–753 (1995).

[10]C. Tegeler, S. C. Strother, J. R. Anderson, and S.-G. Kim, ''Reproducibility of BOLD-based functional MRI obtained at 4T,'' Human Brain Mapping **7**, 267–283 (1999).

[11]J. H. Lee, M. Garwood, R. Menon, G. Adriany, P. Andersen, C. L. Truwit, and K. Ugurbil, ''High contrast and fast three-dimensional magnetic resonance imaging at high fields,'' Magn. Reson. Med. **34**, 308–312 (1995).

[12]R. P. Woods, S. T. Grafton, C. J. Holmes, S. R. Cherry, and J. C. Mazziotta, ''Automated image registration. I. General methods and intrasubject, intramodality validation,'' J. Comput. Assist. Tomogr. **22**, 139–152 (1998).

[13]U. Kjems, S. C. Strother, J. R. Anderson, I. Law, and L. K. Hansen, ''Enhancing the multivariate signal of [^{15}O] water PET studies with a new nonlinear neuroanatomical registration algorithm,'' IEEE Trans. Med. Imag. **18**, 301–319 (1999).

[14]K. Rehm, S. C. Strother, J. R. Anderson, K. A. Schaper, and D. A. Rottenberg, ''Display of merged multimodality brain images using interleaved pixels with independent color scales,'' J. Nucl. Med. **35**, 1815–1821 (1994).

[15]J.-S. Liow, S. C. Strother, K. Rehm, and D. A. Rottenberg, ''Improved resolution for PET volume imaging through three-dimensional iterative reconstruction,'' J. Nucl. Med. **38**, 1623–1631 (1997).

[16]K. J. Worsley, A. C. Evans, S. Marrett, and P. Neelin, ''A three-dimensional statistical analysis for CBF activation studies in human brain,'' J. Cereb. Blood Flow Metab. **12**, 900–918 (1992).

[17]S. C. Strother, N. Lange, J. R. Anderson, K. A. Schaper, K. Rehm, L. K. Hansen, and D. A. Rottenberg, ''Activation pattern reproducibility: Measuring the effects of group size and data analysis models,'' Human Brain Mapping **5**, 312–316 (1997).

[18]S.-G. Kim, J. Ashe, K. Hendrich, J. M. Ellermann, H. Merkle, K. Ugurbil, and A. P. Georgopoulos, ''Functional magnetic resonance imaging of motor cortex: Hemispheric asymmetry and handedness,'' Science **261**, 615–617 (1994).

[19]S. Pajevic, M. E. Daube-Witherspoon, S. L. Bacharach, and R. E. Carson, ''Noise characteristics of 3D and 2D PET images,'' IEEE Trans. Med. Imaging **17**, 9–23 (1998).

[20]D. L. Bailey, M. P. Miller, T. J. Spinks, P. M. Bloomfield, L. Livieratos, R. B. Banati, R. Myers, and T. Jones, ''Brain PET studies with a high sensitivity fully three-dimensional tomograph,'' *Quantitative Functional Brain Imaging with Positron Emission Tomography* (Academic, San Diego, 1998), pp. 25–31.